

Prompt-Guided Image-Adaptive Neural Implicit Lookup Tables for Interpretable Image Enhancement

Satoshi Kosugi

Tokyo Institute of Technology
Yokohama, Kanagawa, Japan
kosugi.s.aa@m.titech.ac.jp

Abstract

In this paper, we delve into the concept of interpretable image enhancement, a technique that enhances image quality by adjusting filter parameters with easily understandable names such as “Exposure” and “Contrast”. Unlike using predefined image editing filters, our framework utilizes learnable filters that acquire interpretable names through training. Our contribution is two-fold. Firstly, we introduce a novel filter architecture called an image-adaptive neural implicit lookup table, which uses a multilayer perceptron to implicitly define the transformation from input feature space to output color space. By incorporating image-adaptive parameters directly into the input features, we achieve highly expressive filters. Secondly, we introduce a prompt guidance loss to assign interpretable names to each filter. We evaluate visual impressions of enhancement results, such as exposure and contrast, using a vision and language model along with guiding prompts. We define a constraint to ensure that each filter affects only the targeted visual impression without influencing other attributes, which allows us to obtain the desired filter effects. Experimental results show that our method outperforms existing predefined filter-based methods, thanks to the filters optimized to predict target results. Our source code is available at <https://github.com/satoshi-kosugi/PG-IA-NILUT>.

CCS Concepts

• **Computing methodologies** → **Image processing; Computational photography.**

Keywords

Image enhancement, Lookup table, Implicit neural representation, Vision and language, CLIP, Interpretability

ACM Reference Format:

Satoshi Kosugi. 2024. Prompt-Guided Image-Adaptive Neural Implicit Lookup Tables for Interpretable Image Enhancement. In *Proceedings of the 32nd ACM International Conference on Multimedia (MM '24)*, October 28–November 1, 2024, Melbourne, VIC, Australia. ACM, New York, NY, USA, 14 pages. <https://doi.org/10.1145/3664647.3680743>

1 Introduction

Image enhancement has become an essential task in modern digital image processing, enhancing the visual quality of images by

adjusting their brightness and color. This process significantly increases an image’s utility across various applications. This paper focuses on image enhancement techniques, examining their scope and potential in detail. Especially, we delve into the concept of interpretable image enhancement, a technique that improves images through the adjustment of filter parameters with easily understandable names, such as “Exposure”, “Contrast”, and “Saturation”. This approach allows the user to adjust the enhancement results according to his or her preference and to learn and more effectively utilize the image enhancement process itself. Consequently, interpretable image enhancement is anticipated to substantially enhance users’ comprehension and manipulation of image processing.

Previous interpretable image enhancement methods [8, 12, 19, 20] employ predefined image editing filters, and convolutional neural networks (CNNs) are trained to determine the optimal parameters for these filters. Since these filters are designed in a manner that is understandable to humans, they facilitate interpretable image enhancement. However, the effectiveness of enhancement may be constrained by the limitations inherent in the design of these predefined filters. For instance, the “Exposure” filter can be designed in various ways, making it challenging to manually craft an optimal Exposure filter for achieving specific results. In contrast, most recent image enhancement methods [18, 29, 30, 33, 34] employ 3D lookup tables (LUTs) [31], which are tables that record input RGB values and corresponding output RGB values. Multiple 3D LUTs are employed to apply various effects, and image-adaptive enhancement is achieved by linearly summing these 3D LUTs, weighted by image-adaptive parameters. Unlike predefined image editing filters, 3D LUTs are learnable filters optimized for predicting enhancement results, enabling high quality enhancement. However, there are two notable issues associated with the use of 3D LUTs. Firstly, the expressive power is limited. This is because the multiple 3D LUTs are merely summed in a linear fashion, weighted by image-adaptive parameters, which means the image-adaptive parameters can only adjust the enhancement effect in a linear manner. Secondly, 3D LUTs lack interpretable names. Since they are optimized solely for predicting target enhancement results, their effects may not be intuitively understood by humans.

To achieve high-performing and interpretable enhancement, we propose learnable and interpretable filters named a Prompt-Guided Image-Adaptive Neural Implicit Lookup Table (PG-IA-NILUT). Our contribution is twofold. Firstly, we introduce a novel learnable filter architecture called an Image-Adaptive Neural Implicit Lookup Table (IA-NILUT). Inspired by a previous method [5], we utilize implicit neural representations [23] for a color transformation. While previous researchers have used 3D LUTs to explicitly record input-output RGB value pairs, we employ a multilayer perceptron (MLP)

MM '24, October 28–November 1, 2024, Melbourne, VIC, Australia

© 2024 Copyright held by the owner/author(s). Publication rights licensed to ACM. This is the author’s version of the work. It is posted here for your personal use. Not for redistribution. The definitive Version of Record was published in *Proceedings of the 32nd ACM International Conference on Multimedia (MM '24)*, October 28–November 1, 2024, Melbourne, VIC, Australia, <https://doi.org/10.1145/3664647.3680743>.

to implicitly define the transformation from input feature space to output color space. The most significant distinction from the 3D LUT-based methods is that we incorporate image-adaptive parameters directly into the input features. Since an MLP can represent nonlinear and complex relationships between inputs and outputs, our approach enables these image-adaptive parameters to exert a complex influence on the output RGB values, thereby achieving highly expressive filter effects. Additionally, to address the problem of high computational costs of MLPs, we introduce the technique called LUT bypassing. Instead of applying the MLP directly to each pixel, we convert the MLP into a 3D LUT, which is then applied to each pixel. Color transformation through the 3D LUT is computationally inexpensive, enabling cost-effective image enhancement.

As a second contribution, we propose a prompt guidance loss to assign interpretable names to each filter. This loss function utilizes CLIP [21], a vision and language model capable of embedding images and text within the same feature space. CLIP has demonstrated its ability to quantify image impressions [25]. For example, for an impression word such as “Exposure,” we prepare pairs of positive and negative prompts (e.g., “Overexposed photo.” and “Underexposed photo.”) and calculate the ratio of the similarities between the image feature and each prompt feature. This allows us to quantitatively evaluate the “Exposure” impression conveyed by the image. In this study, we propose using the pairs of positive and negative prompts as guiding prompts to guide the filters toward achieving the desired effects. Our prompt guidance loss ensures that when the parameter associated with “Exposure” is altered, only the “Exposure” score changes, while the scores for other impressions remain unaffected. By minimizing this prompt guidance loss in conjunction with a reconstruction loss of the target results, we achieve high-performing and interpretable filters.

To evaluate the proposed method, we perform experiments with the FiveK [4] and PPR10K [17] datasets. We show that the proposed method achieves interpretable filters, which are understandable to humans. In addition, the proposed method achieves higher performance than existing predefined filter-based methods.

The contributions of this paper are as follows:

- For interpretable and learnable filters, we develop the IA-NILUT, a highly expressive filter architecture.
- To assign interpretable names to each filter, we introduce the prompt guidance loss.
- The proposed method achieves higher performance than existing predefined filter-based methods.

2 Related Works

2.1 Encoder-Decoder-Based Methods

Early CNN-based image enhancement methods utilized encoder-decoder-based CNNs. Kim et al. [10] developed a sequential approach to image enhancement, applying global and local adjustments in stages. Kim et al. [9] developed a representative color transform technique for improved color accuracy. Zhao et al. [36] explored the use of invertible neural networks to restore content accurately while avoiding bias. Zhang et al. [35] leveraged Transformer [24] for structure-aware enhancement. Recognizing the diversity in user preferences, some researchers have focused on

personalized image enhancement models [11, 14]. Because encoder-decoder-based methods are computationally costly, filter-based approaches have recently become more prevalent.

2.2 Predefined Filter-Based Methods

Predefined filter-based methods train CNNs to predict the parameters of predefined image editing filters. Park et al. [20] employed reinforcement learning to train an agent that iteratively determines the parameters. Hu et al. [8] utilized generative adversarial networks (GANs) to generate more realistic results. Kosugi and Yamasaki [12] reproduced Photoshop filters, enabling more efficient prediction of enhancement results. Bianco et al. [3] and Li et al. [16] used color transformation curve for flexible enhancement. Ouyang et al. [19] achieved local enhancement with region-specific color filters. Some researchers proposed methods for crowd workers to adjust the filter parameters [13, 15]. These methods can achieve interpretable enhancements because the predefined filters are named in a way that is understandable to humans, but the enhancement performance can be limited by the design of these predefined filters.

2.3 Learnable Filter-Based Methods

Learnable filter-based methods optimize the filters using training data. He et al. [6] successfully replicated an image editing process using an MLP. Wang et al. [27] further enhanced these results by applying sequential image retouching.

Recent learnable filter-based methods largely use 3D LUTs, which are trainable tables that map input RGB values to corresponding output values. Zeng et al. [31] utilized multiple 3D LUTs, combining them with image-adaptive weights. Wang et al. [26] introduced spatial-aware 3D LUTs. Yang et al. [29] made the sampling points of 3D LUTs adapt to images. Yang et al. [30] incorporated a 1D LUT alongside 3D LUTs. Zhang et al. [33] proposed a compressed representation of 3D LUTs to efficiently increase their number. Zhang et al. [34] introduced hashing techniques to reduce parameters. Liu et al. [18] defined 4D LUTs for local enhancement. Shi et al. [22] developed a network that considers cross attention between RGB values and LUTs. Zhang et al. [32] combined 3D LUTs with local laplacian filters [2] for advanced effects. Despite the high performance, they lack interpretability, presenting a challenge for understanding the modifications they make to the images.

3 Preliminary

This section describes the key existing method: image-adaptive 3D LUTs [31]. 3D LUTs are learnable tables that record input RGB values and the corresponding output RGB values. We denote the matrix representing the sampling points by $\mathbf{I} \in \mathbb{R}^{N^3 \times 3}$ and the matrix recording the corresponding output values by $\mathbf{O} \in \mathbb{R}^{N^3 \times 3}$, where N is the number of sampling coordinates. Given an input RGB value of $[r^x, g^x, b^x]$, an index s is searched for such that the vector in the s -th row of \mathbf{I} matches $[r^x, g^x, b^x]$; then, the s -th row of \mathbf{O} , denoted as $[r^y, g^y, b^y]$, is returned. If the input RGB value is not included in \mathbf{I} , an interpolated value is returned based on the surrounding RGB values. This process is performed on all pixels. Let \mathbf{X} and \mathbf{Y} be input and output images, respectively, the transformation is represented as $\mathbf{Y} = \text{Lookup}(\mathbf{X}, \{\mathbf{I}, \mathbf{O}\})$.

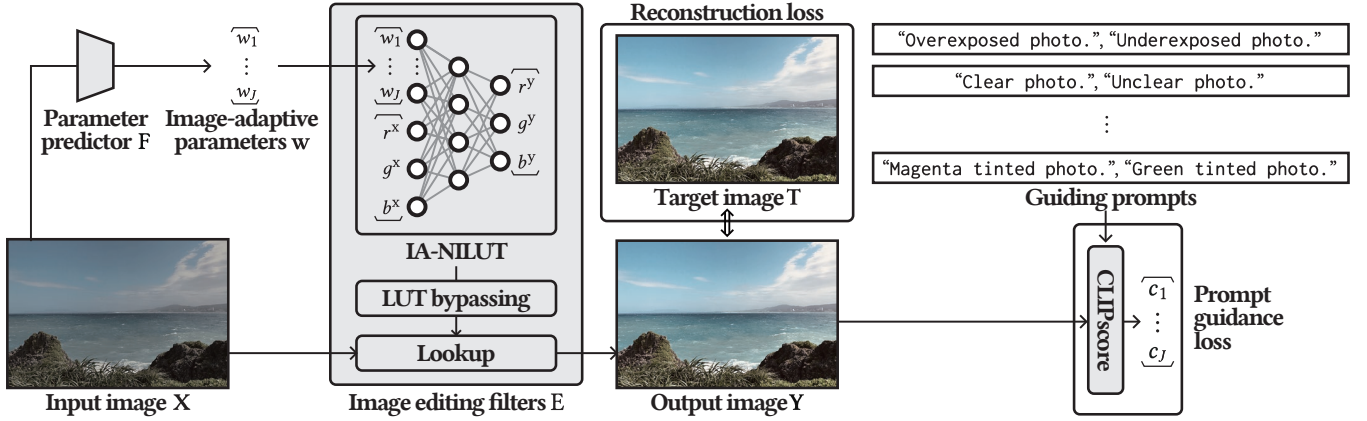


Figure 1: Overview of our interpretable image enhancement method. For a highly expressive filter architecture, we propose an IA-NILUT. By employing LUT bypassing, we can expedite the transformation process. Additionally, we introduce a prompt guidance loss to assign interpretable names to each filter. As our method provides an interpretable and learnable framework for enhancement, it outperforms other predefined filter-based methods in terms of performance.

In image-adaptive 3D LUTs [31], multiple LUTs $\{I, O_1\}, \dots, \{I, O_J\}$ are employed for different effects. To achieve optimal enhancement for each image, image-adaptive parameters $\mathbf{w} \in \mathbb{R}^J$ are used to weight each LUT. The enhanced result is represented as

$$Y = \text{Lookup}(X, \{I, O_1\}) \times w_1 + \dots + \text{Lookup}(X, \{I, O_J\}) \times w_J. \quad (1)$$

Each $\text{Lookup}(X, \{I, O_j\})$ can be regarded as the result of applying different filters to X , and each w_j works as a filter parameter that determines the strength of the filter effect. O_1, \dots, O_J can be optimized to predict enhancement results, which makes the lookup tables as efficient image editing filters. Because pixels are transformed independently, Eq. (1) can be simplified as

$$Y = \text{Lookup}(X, \{I, O_1 \times w_1 + \dots + O_J \times w_J\}). \quad (2)$$

The image-adaptive parameters \mathbf{w} are predicted by CNN-based parameter predictor F as $\mathbf{w} = F(X)$. The parameter predictor F processes images that are downscaled to a fixed size, and Lookup function operates quickly. As a result, this framework enables real-time enhancement for images of any size.

This approach faces two main issues. First, there’s the issue of limited expressive power. The enhancement results are summed linearly as shown in Eq. (1), meaning that image-adaptive parameters cannot produce complex effects. Second, the 3D LUTs lack interpretable names. Since the 3D LUTs are optimized solely for predicting target results, there’s no assurance that their effects will be meaningful or understandable to humans. We address these challenges by introducing highly expressive and interpretable filters.

4 Proposed Method

To achieve high-performing and interpretable enhancement, we make two contributions. First, we propose a novel filter architecture called an IA-NILUT. Second, we introduce a prompt guidance loss to give interpretable names to each filter. We show the overview in Figure 1 and describe the contributions in the following sections.

4.1 IA-NILUT

We propose a novel filter architecture called an IA-NILUT. Inspired by the existing method known as NILUTs [5], our approach employs an implicit neural representation [23], wherein we implicitly define the transformation from input space to output space using an MLP. We visualize the difference between the 3D LUTs and our IA-NILUT in Figure 2. The most significant distinction between the previous image-adaptive 3D LUTs and our IA-NILUT is that the IA-NILUT incorporates the image-adaptive parameters directly into the input features. Given that an MLP is capable of capturing nonlinear and intricate relationships between input and output variables, our method allows the image-adaptive parameters to intricately affect the output RGB values, thereby achieving highly expressive filter effects. We define the color transformation process as follows,

$$\begin{aligned} [r^y, g^y, b^y] &= [r^x, g^x, b^x] \\ &+ e([r^x, g^x, b^x] \oplus \text{sort}([r^x, g^x, b^x]) \oplus \mathbf{w}) \\ &- e([r^x, g^x, b^x] \oplus \text{sort}([r^x, g^x, b^x]) \oplus \mathbf{0}), \end{aligned} \quad (3)$$

where e represents the MLP, and \oplus denotes vector concatenation. We make two improvements to the color transformation. First, we use the sorted RGB values, which are denoted by $\text{sort}([r^x, g^x, b^x])$, because they play an important role in filter interpretability. For instance, in the HSV color space, saturation is determined by the maximum and minimum RGB values. Second, we add the difference between $e([r^x, g^x, b^x] \oplus \text{sort}([r^x, g^x, b^x]) \oplus \mathbf{w})$ and $e([r^x, g^x, b^x] \oplus \text{sort}([r^x, g^x, b^x]) \oplus \mathbf{0})$ into the input RGB values. This ensures that the original RGB values are retained in the output when \mathbf{w} is set to $\mathbf{0}$, a common characteristic of image editing filters. We define \hat{E} as a function that applies Eq. (3) to each pixel of image X , and the image transformation process is represented as follows:

$$Y = \hat{E}(X, \mathbf{w}). \quad (4)$$

LUT bypassing. Since MLPs involve multiple nonlinear transformations, the computational cost is significant, especially when processing large sized images. To address this issue, we propose

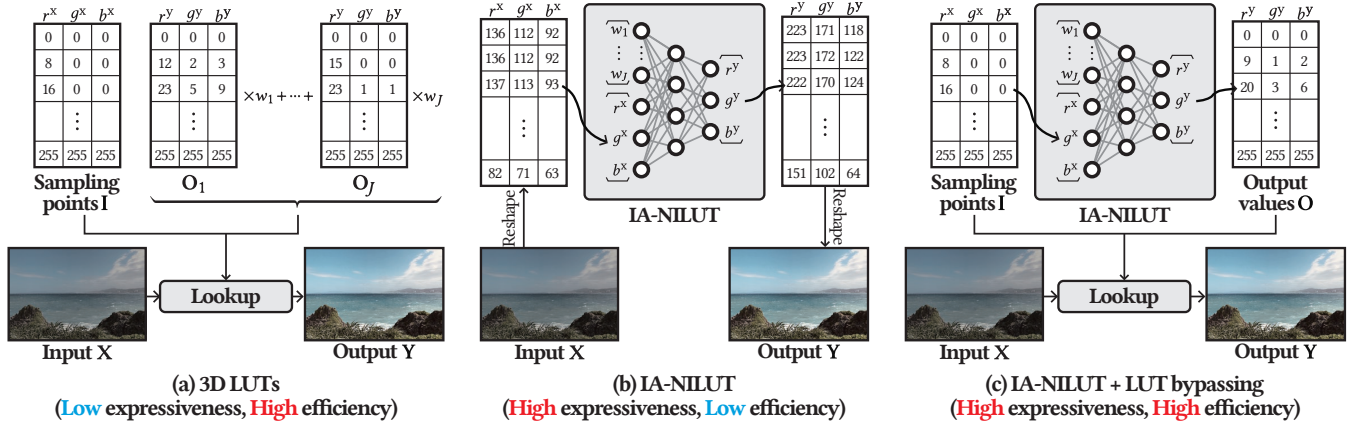


Figure 2: Comparison between the 3D LUTs [31], the IA-NILUT, and the IA-NILUT with the LUT bypassing.

LUT bypassing. Instead of directly applying the MLP to every pixel of the image, we convert the MLP into an LUT and apply this LUT to the image as shown in Figure 2(c). Eq. (4) is transformed as follows,

$$Y = E(X, \mathbf{w}) = \text{Lookup}(X, \{\mathbf{I}, \mathbf{O}\}), \quad (5)$$

where $\mathbf{O} = \hat{E}(\mathbf{I}, \mathbf{w})$.

The sampling points $\mathbf{I} \in \mathbb{R}^{N^3 \times 3}$ are considered as an image with N^3 pixels. This is then converted into \mathbf{O} by the MLP. Following this conversion, the input image X is transformed using the lookup table comprising pairs of \mathbf{I} and \mathbf{O} . In our experiment, we set N to 33, which results in \mathbf{I} being treated as an image composed of 35,937 pixels. For comparison, a 512×512 image contains 262,144 pixels, indicating that \mathbf{I} represents a relatively small image. Even when processing large-sized images, the MLP is applied only to \mathbf{I} , which means that the computational cost of the MLP remains constant. LUT bypassing leverages the expressive power of MLPs while also benefiting from the low computational cost associated with LUTs.

Comparison with advanced LUT-based methods. Recent researchers have made various improvements to LUTs to enhance their expressiveness. For example, AdaInt [29] makes the sampling points \mathbf{I} to be image-adaptive. CLUTNet [33] uses a compressed representation of 3D LUTs. The most significant difference between our method and these existing methods lies in the number of image-adaptive parameters. The existing methods improve expressiveness by increasing the number of image-adaptive parameters; for example, AdaInt and CLUTNet use 99 and 20 image-adaptive parameters, respectively. However, this approach makes interpretability more complex. Too many parameters can make the image editing process confusing for users. In contrast, our method boosts expressiveness by using an implicit neural representation, without increasing the number of image-adaptive parameters. In our experiments, we use only five image-adaptive parameters. This results in a filter architecture that’s easier to understand.

4.2 Prompt Guidance Loss

We introduce a prompt guidance loss that assigns interpretable names to each filter. In this loss function, we utilize CLIP [21], a

vision and language model that embeds images and text within the same feature space. CLIP has demonstrated its ability to quantitatively assess visual impressions [25]. When evaluating an image’s “Exposure,” we create pairs of prompts that contrast positive and negative aspects, such as “Overexposed photo.” versus “Underexposed photo.” We denote the similarities between the image feature and each prompt feature as s^+ and s^- , respectively. The image’s Exposure impression can be evaluated using the formula $\exp(s^+) / (\exp(s^+) + \exp(s^-))$.

We propose using the pairs of positive and negative prompts as guiding prompts to guide the filters toward achieving the desired effects. We illustrate our motivation in Figure 3. We prepare J filter names along with pairs of corresponding guiding prompts, assigning a filter name to each dimension of the J -dimensional image-adaptive parameters \mathbf{w} . During the training phase, we assess the impressions of the enhanced results with each guiding prompt. When we assign the filter name “Exposure” to w_1 , we expect that a change in w_1 will only affect the Exposure score, without impacting other scores such as “Contrast” or “Saturation” as shown in Figure 3(b). If the Contrast and Saturation scores change as shown in Figure 3(c), this could be considered undesired behavior for the Exposure filter, potentially confusing users. Therefore, we propose a constraint that ensures only specific scores are affected when parameters are altered, while other scores remain unchanged.

We define randomly sampled weights as $\bar{\mathbf{w}}$, and denote the scores $\mathbf{c} \in \mathbb{R}^J$ evaluated on J prompt pairs as follows.

$$\mathbf{c} = \text{CLIPscore}(E(X, \bar{\mathbf{w}})). \quad (6)$$

To ensure that a specific filter effect is applied when w_j is altered, we define the prompt guidance loss. Instead of adding Δw_j to \bar{w}_j , we directly apply a constraint to the gradient in the following way.

$$\mathcal{L}_{\text{PG}} = \sum_{j=1}^J \left(\lambda_j \left| \frac{\partial c_j}{\partial w_j} - 1 \right| + \lambda \sum_{j' \neq j} \left| \frac{\partial c_{j'}}{\partial w_j} - 0 \right| \right), \quad (7)$$

where λ_j and λ are hyperparameters. This constraint guarantees that w_j affects only the targeted score c_j , while the remaining scores $c_{j'} (j' \neq j)$ are unaffected. By minimizing \mathcal{L}_{PG} , we can assign interpretable names to each filter.

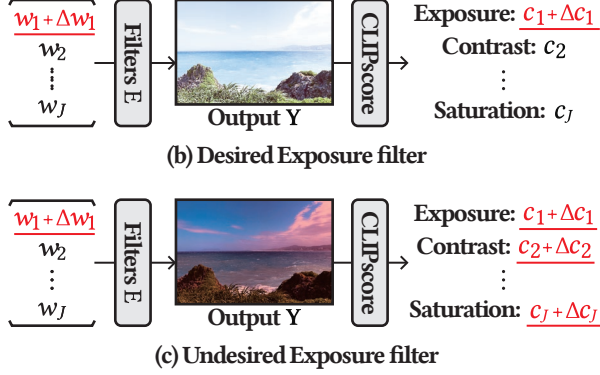
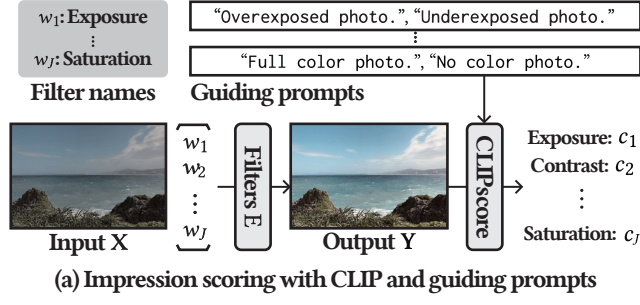


Figure 3: Motivation for our prompt guidance loss.

4.3 Training and Testing

The pairs of input and target images for training are denoted as $\{X_1, T_1\}, \dots, \{X_J, T_J\}$. We divide the training steps into three stages. In the first training stage, only the filters E are trained, using only the prompt guidance loss \mathcal{L}_{PG} .

$$E = \operatorname{argmin}_E \mathcal{L}_{PG}. \quad (8)$$

In the second stage, we introduce image-adaptive parameters w_1, \dots, w_J for images X_1, \dots, X_J . The training process is defined as

$$E, w_1, \dots, w_J = \operatorname{argmin}_{E, w_1, \dots, w_J} \mathcal{L}_{PG} + \sum_{i=1}^J \operatorname{MSE}(T_i, E(X_i, w_i)) + \sum_{i=1}^J \operatorname{MSE}(X_i, E(T_i, -w_i)), \quad (9)$$

where MSE represents the mean squared error function. The third term is a constraint ensuring that the input image is reconstructed from the target image when the parameters w_i are reversed, a property that existing filters also possess. In the final stage, the parameter predictor F is trained as

$$F = \operatorname{argmin}_F \sum_{i=1}^J \operatorname{MSE}(T_i, E(X_i, F(X_i))). \quad (10)$$

At test time, the enhancement results are generated using the trained E and F , as $Y = E(X, F(X))$. The filters E can achieve fast transformations through the LUT bypassing, and the parameter predictor F resizes the input image to a fixed resolution before processing, resulting in real-time enhancement.

Table 1: Guiding prompts.

	Filter name	Positive prompt	Negative prompt
w_1	Exposure	“Overexposed photo.”	“Underexposed photo.”
	(FiveK) Contrast	“Clear photo.”	“Unclear photo.”
w_2	(PPR10K) Contrast	“High contrast photo.”	“Low contrast photo.”
w_3	Saturation	“Full color photo.”	“No color photo.”
w_4	Color temperature	“Yellow tinted photo.”	“Blue tinted photo.”
w_5	Tint correction	“Magenta tinted photo.”	“Green tinted photo.”

5 Experiments

5.1 Datasets and Implementation

We utilize two widely used datasets: FiveK [4] and PPR10K [17]. FiveK contains 5,000 images, each retouched by five experts. Following the setting of previous papers [29, 33], we use 4,500 of these images for training and the remaining 500 for testing, employing the images retouched by Expert C as the target images. We conduct experiments in both 480p resolution (where the shorter side is resized to 480 pixels) and the original 4K resolution. To train efficiently, we perform the training at 480p resolution and use the original 4K resolution only for testing. PPR10K includes 11,161 portrait images, each retouched by three experts. We conduct our experiments using the results retouched by Expert A. According to the official setup, we have 8,875 pairs for training and 2,286 pairs for testing. All images are used in a resized format at 360p. We evaluate each method using PSNR, SSIM [28], and the L2-distance in CIE LAB color space (ΔE_{ab}). When measuring runtime, we use the NVIDIA RTX A6000 GPU. Our experiments are based on MMEediting toolbox [1].

In the IA-NILUT, we employ an MLP consisting of five fully connected layers. The hidden features within this MLP are 256-dimensional, and we utilize the hyperbolic tangent as our activation function. For the parameter predictor F , a five-layer CNN is used on FiveK, and ResNet18 [7] is applied to PPR10K, following the configurations reported in previous studies [17, 29].

Inspired by the basic filters in Adobe Lightroom, we define five filter names and employ five corresponding guiding prompt pairs as outlined in Table 1. For the Contrast filter, we use different prompts for each dataset, tailoring them to achieve the desired effects.

5.2 Visualization of Filter Effects

To demonstrate that the proposed method achieves interpretable filter effects, we visualize filter effects in Figure 4. In these visualizations, only certain parameters are varied while others are held constant at 0. These results indicate that each filter produces a specific effect associated with the corresponding guiding prompts. Figure 5 shows examples of sequential application of predicted parameters, where the enhancement process is visualized in a way that is easy for humans to understand. The sequential application of the filter effects in Figure 5 is for visualization purposes only, and the all filter effects are applied simultaneously in practice.

5.3 Ablation Studies

Filter architecture. We use the IA-NILUT for a highly expressive filter architecture. To assess the significance of the IA-NILUT, we train 3D LUTs [31] instead of the IA-NILUT using the prompt

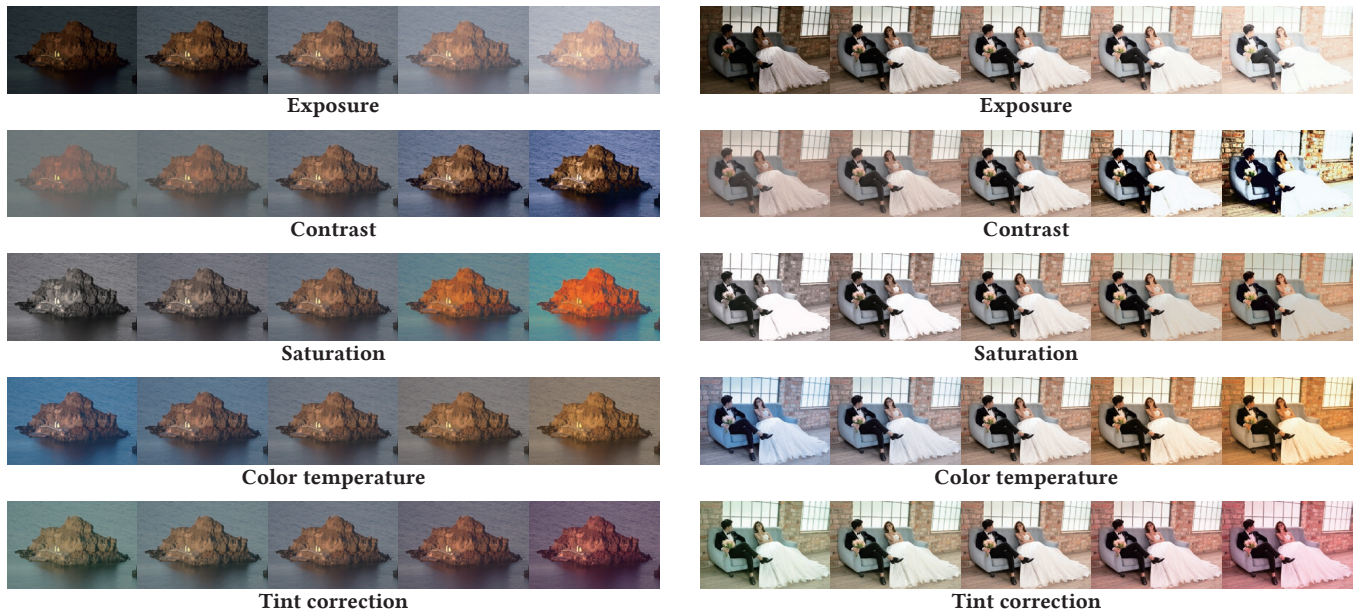


Figure 4: Visualization of learned filter effects. Only certain parameters are varied while others are held constant at 0. The images on the left and right are samples from FiveK and PPR10K, respectively.

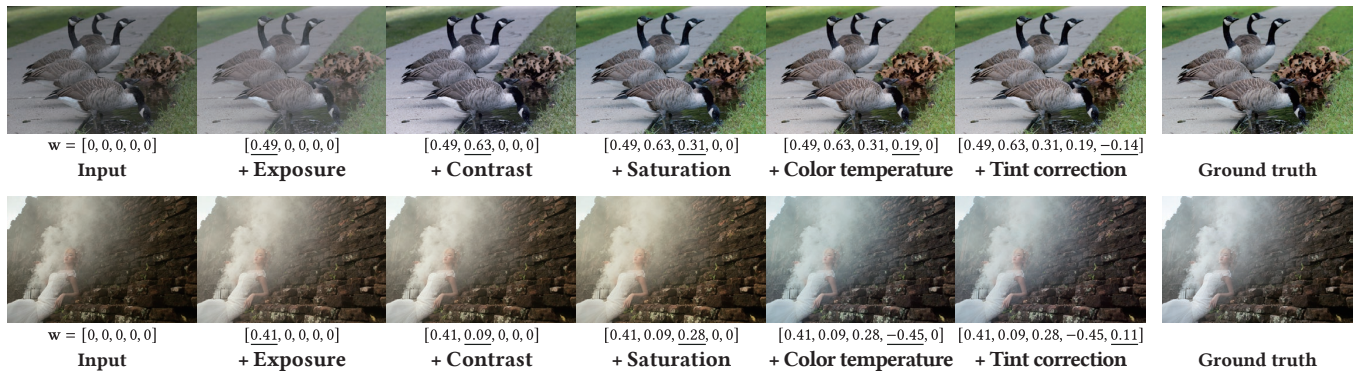


Figure 5: Sequential application of predicted parameters. This sequential application is for visualization purposes only, and the all effects are applied simultaneously in practice. The top and bottom images are samples from FiveK and PPR10K, respectively.

guidance loss. To ensure the original image is preserved when w is set to 0, we modify Eq. (1) as follows,

$$Y = X + \text{Lookup}(X, \{\mathbf{I}, \mathbf{O}_1\}) \times w_1 + \dots + \text{Lookup}(X, \{\mathbf{I}, \mathbf{O}_J\}) \times w_J. \quad (11)$$

As shown in Table 2, the IA-NILUT achieves higher performance, indicating the higher expressive power of the IA-NILUT. The filter effects of the 3D LUTs trained with the prompt guidance loss are shown in Figure 6. The desired filter effects are not achieved, indicating that the IA-NILUT is essential for interpretable filters.

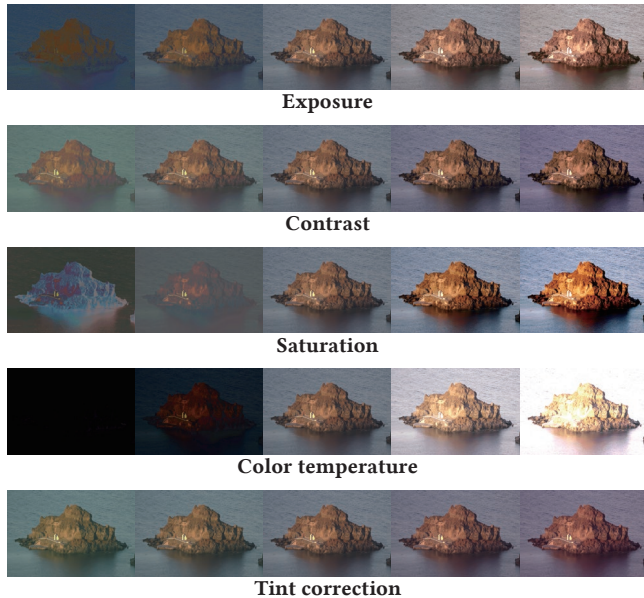
LUT bypassing. We use the LUT bypassing to reduce the computational cost. To demonstrate the effectiveness of the LUT bypassing, we present a comparison of PSNR and runtime in Table 3, and a comparison of the required GPU memory in Figure 7. When processing some 4K images that require more memory than the available limit

in Table 3, we divide the image into four patches and sequentially apply the MLP to each patch. Given that an MLP is computationally intensive, the absence of the LUT bypassing leads to increased computational costs, particularly when processing large-sized images. In contrast, by employing the LUT bypassing, the MLP is only applied to sampling points, the size of which are independent of the overall image size. In addition, the LUT bypassing has little effect on the PSNR. This approach leads to computationally efficient enhancement that is nearly unaffected by the image size.

Prompt guidance loss. We employ the prompt guidance loss to assign interpretable names to each filter. To demonstrate the significance of the prompt guidance loss, we present the effects of filters when training the IA-NILUT without this loss in Figure 8. It is difficult to assign interpretable names to these filters. For instance, the first filter influences both exposure and color simultaneously.

Table 2: Comparison of filter architecture using FiveK (480p).

Method	PSNR \uparrow	SSIM \uparrow	$\Delta E_{ab}\downarrow$
3D LUTs [31] w/ prompt guidance loss	24.92	0.924	8.23
IA-NILUT w/ prompt guidance loss	25.22	0.930	7.76

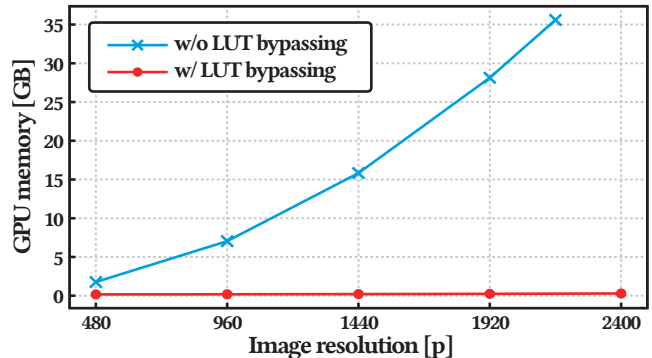
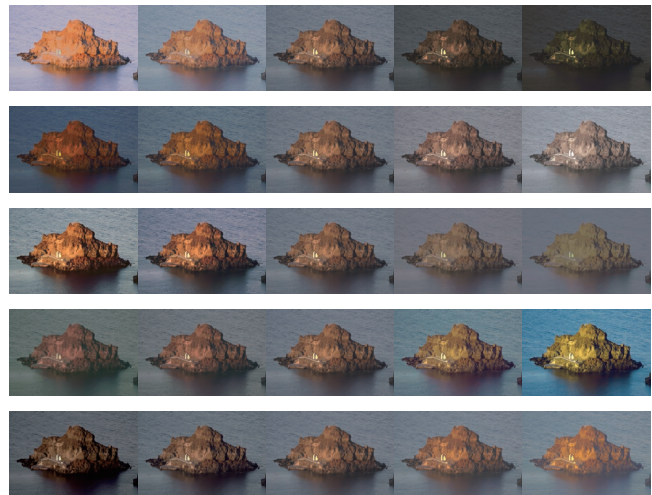

Figure 6: Filter effects of 3DLUTs [31] trained with the prompt guidance loss.
Table 3: Effectiveness of the LUT bypassing on FiveK.

Method	480p		Full Res. (4K)	
	PSNR \uparrow	Runtime \downarrow	PSNR \uparrow	Runtime \downarrow
Ours w/o LUT bypassing	25.22	1.9 ms	25.06	7.8 ms
Ours w/ LUT bypassing	25.22	1.9 ms	25.05	2.0 ms

Similarly, the second filter affects exposure and saturation together, while the fourth filter impacts color and contrast at the same time. Both the third and fifth filters are able to modify the image’s contrast; if both filters had the same “Contrast” name, users would be confused. These results highlight the prompt guidance loss’s critical role to assign interpretable names to each filter.

5.4 Comparison with the State-of-the-Arts

We employ four interpretable methods: D&R [20], Exposure [8], UIE [12], and RSFNet [19]. For a fair comparison, we utilize only the filters adopted in these methods and apply the same parameter predictor as ours. For the filters from UIE, we exclude non-differentiable filters. Additionally, we include three uninterpretable methods: our baseline method (3D LUTs [31]), and the two state-of-the-art methods (AdaInt [29] and CLUTNet [33]). Since the pre-trained weights for CLUTNet with PPR10K are not publicly available, we only show the performance on FiveK. The performance of these


Figure 7: Required GPU memory w/ and w/o LUT bypassing.

Figure 8: Filter effects of the IA-NILUT without the prompt guidance loss.

uninterpretable methods is provided solely for reference, as our primary focus is on interpretable image enhancement.

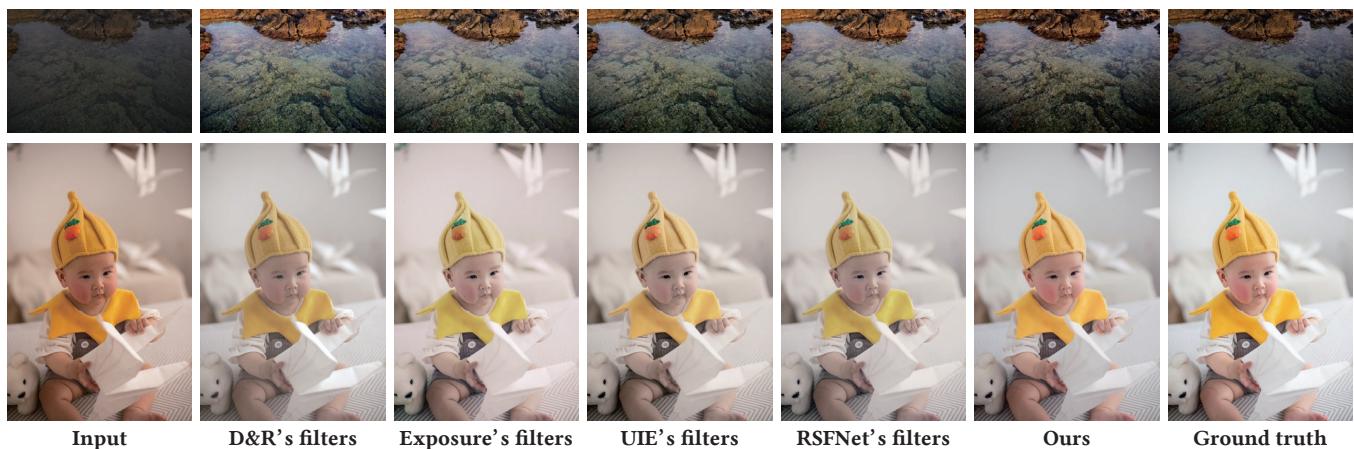
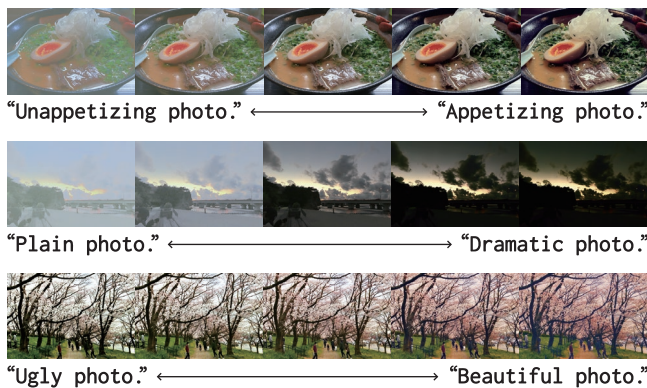
We present quantitative comparisons in Table 4 and visual comparisons with other interpretable methods in Figure 9. Because our filters are learnable and optimized to predict the ground truth, our method achieves better performance than other predefined filter-based methods. While the runtime for Exposure’s filters and UIE’s filters is long due to their complex color transformations, the runtime of our method is almost unaffected by the image size thanks to the LUT bypassing. Our method achieves comparable performance to that of uninterpretable methods on some metrics. These results highlight the potential of our method to bridge the gap between interpretability and high performance.

5.5 Various Filter Effects

By using different guiding prompts, we can achieve various filter effects. In addition to the guiding prompts listed in Table 1, we assign additional guiding prompts to w_6 and then train the filters using only the prompt guidance loss. Figure 10 displays examples of some guiding prompts and their corresponding filter effects. Our

Table 4: Quantitative comparisons on (a) FiveK and (b) PPR10K. The top three methods are uninterpretable methods, while the bottom five are interpretable methods.

Method	(a) FiveK				(b) PPR10K						
	480p				Full Resolution (4K)				360p		
	PSNR \uparrow	SSIM \uparrow	$\Delta E_{ab}\downarrow$	Runtime \downarrow	PSNR \uparrow	SSIM \uparrow	$\Delta E_{ab}\downarrow$	Runtime \downarrow	PSNR \uparrow	SSIM \uparrow	$\Delta E_{ab}\downarrow$
3DLUTs [31]	25.36	0.927	7.56	1.5 ms	25.32	0.933	7.61	1.5 ms	26.29	0.961	6.58
AdaInt [29]	25.50	0.930	7.47	1.5 ms	25.50	0.935	7.46	1.5 ms	26.29	0.961	6.59
CLUTNet [33]	25.55	0.931	7.50	1.9 ms	25.50	0.935	7.53	2.1 ms	-	-	-
D&R’s filters [20]	23.86	0.903	9.07	1.9 ms	23.76	0.907	9.16	1.9 ms	24.27	0.934	8.11
Exposure’s filters [8]	25.04	0.920	7.83	4.3 ms	24.91	0.924	7.92	15.9 ms	25.53	0.954	7.55
UIE’s filters [12]	24.74	0.923	8.06	5.0 ms	24.61	0.928	8.14	58.9 ms	25.45	0.956	7.53
RSFNet’s filters [19]	24.86	0.924	7.89	2.8 ms	24.82	0.928	7.96	2.8 ms	25.41	0.946	7.48
PG-IA-NILUT (ours)	25.22	0.930	7.76	1.9 ms	25.05	0.934	7.88	2.0 ms	26.00	0.957	6.81

**Figure 9: Visual comparisons of interpretable methods, with the top image from FiveK and the bottom from PPR10K.****Figure 10: Filter effects by various guiding prompts.**

filter is highly expressive, enabling us to achieve various effects and demonstrating its practical utility for image editing applications.

6 Limitation

Although our method achieves interpretable and high-performing enhancement, it encounters a drawback where the use of the prompt

Table 5: Impact of the prompt guidance loss on FiveK.

Method	PSNR \uparrow	SSIM \uparrow	$\Delta E_{ab}\downarrow$
Ours w/o prompt guidance loss	25.46	0.930	7.60
Ours w/ prompt guidance loss	25.22	0.930	7.76

guidance loss slightly deteriorates performance as shown in Table 5. A potential approach to improve performance while preserving interpretability involves refining the selection of the guiding prompts. We selected the prompts listed in Table 1 heuristically; however, it remains uncertain whether they are optimal for both interpretability and performance. The development of an automatic prompt selection mechanism is identified as an avenue for future research.

7 Conclusion

In this paper, we explored interpretable image enhancement. We proposed a highly expressive filter architecture named an IA-NILUT. Additionally, we introduced the prompt guidance loss to assign interpretable names to each filter. Our experiments demonstrated that our method not only provides interpretability but also achieves higher performance compared to existing interpretable filters.

Acknowledgments

A part of this research was supported by JSPS KAKENHI Grant Number 23K19997.

References

- [1] 2020-08-31. <https://github.com/open-mmlab/mmediting>
- [2] Mathieu Aubry, Sylvain Paris, Samuel W Hasinoff, Jan Kautz, and Frédo Durand. 2014. Fast local laplacian filters: Theory and applications. *ACM Transactions on Graphics* 33, 5 (2014), 1–14.
- [3] Simone Bianco, Claudio Cusano, Flavio Piccoli, and Raimondo Schettini. 2020. Personalized image enhancement using neural spline color transforms. *IEEE Transactions on Image Processing* 29 (2020), 6223–6236.
- [4] Vladimir Bychkovsky, Sylvain Paris, Eric Chan, and Frédo Durand. 2011. Learning photographic global tonal adjustment with a database of input/output image pairs. In *Proceedings of the IEEE Conference on Computer Vision and Pattern Recognition*. 97–104.
- [5] Marcos V Conde, Javier Vazquez-Corral, Michael S Brown, and Radu Timofte. 2024. Nilut: Conditional neural implicit 3d lookup tables for image enhancement. In *Proceedings of the AAAI Conference on Artificial Intelligence*, Vol. 38. 1371–1379.
- [6] Jingwen He, Yihao Liu, Yu Qiao, and Chao Dong. 2020. Conditional sequential modulation for efficient global image retouching. In *Proceedings of the European Conference on Computer Vision*. 679–695.
- [7] Kaiming He, Xiangyu Zhang, Shaoqing Ren, and Jian Sun. 2016. Deep residual learning for image recognition. In *Proceedings of the IEEE conference on computer vision and pattern recognition*. 770–778.
- [8] Yuanming Hu, Hao He, Chenxi Xu, Baoyuan Wang, and Stephen Lin. 2018. Exposure: A white-box photo post-processing framework. *ACM Transactions on Graphics* 37, 2 (2018), 1–17.
- [9] Hanul Kim, Su-Min Choi, Chang-Su Kim, and Yeong Jun Koh. 2021. Representative Color Transform for Image Enhancement. In *Proceedings of the IEEE/CVF International Conference on Computer Vision*. 4459–4468.
- [10] Han-Ul Kim, Young Jun Koh, and Chang-Su Kim. 2020. Global and Local Enhancement Networks for Paired and Unpaired Image Enhancement. In *Proceedings of the European Conference on Computer Vision*.
- [11] Han-Ul Kim, Young Jun Koh, and Chang-Su Kim. 2020. PieNet: Personalized image enhancement network. In *Proceedings of the European Conference on Computer Vision*. 374–390.
- [12] Satoshi Kosugi and Toshihiko Yamasaki. 2020. Unpaired image enhancement featuring reinforcement-learning-controlled image editing software. In *Proceedings of the AAAI Conference on Artificial Intelligence*, Vol. 34. 11296–11303.
- [13] Satoshi Kosugi and Toshihiko Yamasaki. 2023. Crowd-Powered Photo Enhancement Featuring an Active Learning Based Local Filter. *IEEE Transactions on Circuits and Systems for Video Technology* 33, 7 (2023), 3145–3158.
- [14] Satoshi Kosugi and Toshihiko Yamasaki. 2024. Personalized Image Enhancement Featuring Masked Style Modeling. *IEEE Transactions on Circuits and Systems for Video Technology* 34, 1 (2024), 140–152.
- [15] Yuki Koyama, Issei Sato, Daisuke Sakamoto, and Takeo Igarashi. 2017. Sequential line search for efficient visual design optimization by crowds. *ACM Transactions on Graphics (TOG)* 36, 4 (2017), 1–11.
- [16] Chongyi Li, Chunle Guo, Shangchen Zhou, Qiming Ai, Ruicheng Feng, and Chen Change Loy. 2023. FlexiCurve: Flexible Piecewise Curves Estimation for Photo Retouching. In *Proceedings of the IEEE/CVF Conference on Computer Vision and Pattern Recognition Workshops*. 1092–1101.
- [17] Jie Liang, Hui Zeng, Miaomiao Cui, Xuansong Xie, and Lei Zhang. 2021. Ppr10k: A large-scale portrait photo retouching dataset with human-region mask and group-level consistency. In *Proceedings of the IEEE/CVF Conference on Computer Vision and Pattern Recognition*. 653–661.
- [18] Chengxu Liu, Huan Yang, Jianlong Fu, and Xueming Qian. 2023. 4D LUT: learnable context-aware 4d lookup table for image enhancement. *IEEE Transactions on Image Processing* 32 (2023), 4742–4756.
- [19] Wenqi Ouyang, Yi Dong, Xiaoyang Kang, Peiran Ren, Xin Xu, and Xuansong Xie. 2023. RSNNet: A White-Box Image Retouching Approach using Region-Specific Color Filters. In *Proceedings of the IEEE/CVF International Conference on Computer Vision*. 12160–12169.
- [20] Jongchan Park, Joon-Young Lee, Donggeun Yoo, and In So Kweon. 2018. Distort-and-recover: Color enhancement using deep reinforcement learning. In *Proceedings of the IEEE Conference on Computer Vision and Pattern Recognition*. 5928–5936.
- [21] Alec Radford, Jong Wook Kim, Chris Hallacy, Aditya Ramesh, Gabriel Goh, Sandhini Agarwal, Girish Sastry, Amanda Askell, Pamela Mishkin, Jack Clark, et al. 2021. Learning transferable visual models from natural language supervision. In *International Conference on Machine Learning*. 8748–8763.
- [22] Tengfei Shi, Chenglizhao Chen, Yuanbo He, Wenfeng Song, and Aimin Hao. 2023. RGB and LUT based Cross Attention Network for Image Enhancement. In *The British Machine Vision Conference*.
- [23] Vincent Sitzmann, Julien Martel, Alexander Bergman, David Lindell, and Gordon Wetzstein. 2020. Implicit neural representations with periodic activation functions. *Advances in neural information processing systems* 33 (2020), 7462–7473.
- [24] Ashish Vaswani, Noam Shazeer, Niki Parmar, Jakob Uszkoreit, Llion Jones, Aidan N Gomez, Łukasz Kaiser, and Illia Polosukhin. 2017. Attention is all you need. *Advances in neural information processing systems* 30 (2017).
- [25] Jianyi Wang, Kelvin CK Chan, and Chen Change Loy. 2023. Exploring clip for assessing the look and feel of images. In *Proceedings of the AAAI Conference on Artificial Intelligence*, Vol. 37. 2555–2563.
- [26] Tao Wang, Yong Li, Jingyang Peng, Yipeng Ma, Xian Wang, Fenglong Song, and Youliang Yan. 2021. Real-time image enhancer via learnable spatial-aware 3d lookup tables. In *Proceedings of the IEEE/CVF International Conference on Computer Vision*. 2471–2480.
- [27] Yili Wang, Xin Li, Kun Xu, Dongliang He, Qi Zhang, Fu Li, and Errui Ding. 2022. Neural Color Operators for Sequential Image Retouching. In *Proceedings of the European Conference on Computer Vision*. 38–55.
- [28] Zhou Wang, Alan C Bovik, Hamid R Sheikh, and Eero P Simoncelli. 2004. Image quality assessment: from error visibility to structural similarity. *IEEE transactions on image processing* 13, 4 (2004), 600–612.
- [29] Canqian Yang, Meiguang Jin, Xu Jia, Yi Xu, and Ying Chen. 2022. AdaInt: Learning Adaptive Intervals for 3D Lookup Tables on Real-time Image Enhancement. In *Proceedings of the IEEE/CVF Conference on Computer Vision and Pattern Recognition*. 17522–17531.
- [30] Canqian Yang, Meiguang Jin, Yi Xu, Rui Zhang, Ying Chen, and Huaida Liu. 2022. SepLUT: Separable Image-Adaptive Lookup Tables for Real-Time Image Enhancement. In *Proceedings of the European Conference on Computer Vision*. 201–217.
- [31] Hui Zeng, Jianrui Cai, Lida Li, Zisheng Cao, and Lei Zhang. 2022. Learning Image-Adaptive 3D Lookup Tables for High Performance Photo Enhancement in Real-Time. *IEEE Transactions on Pattern Analysis & Machine Intelligence* 44, 04 (2022), 2058–2073.
- [32] Feng Zhang, Ming Tian, Zhiqiang Li, Bin Xu, Qingbo Lu, Changxin Gao, and Nong Sang. 2024. Lookup Table meets Local Laplacian Filter: Pyramid Reconstruction Network for Tone Mapping. *Advances in Neural Information Processing Systems* 36 (2024).
- [33] Fengyi Zhang, Hui Zeng, Tianjun Zhang, and Lin Zhang. 2022. Clut-net: Learning adaptively compressed representations of 3dluts for lightweight image enhancement. In *Proceedings of the 30th ACM International Conference on Multimedia*. 6493–6501.
- [34] Fengyi Zhang, Lin Zhang, Tianjun Zhang, and Dongqing Wang. 2023. Adaptively Hashing 3DLUTs for Lightweight Real-time Image Enhancement. In *IEEE International Conference on Multimedia and Expo*. 2771–2776.
- [35] Zhaoyang Zhang, Yitong Jiang, Jun Jiang, Xiaogang Wang, Ping Luo, and Jinwei Gu. 2021. STAR: A Structure-Aware Lightweight Transformer for Real-Time Image Enhancement. In *Proceedings of the IEEE/CVF International Conference on Computer Vision*. 4106–4115.
- [36] Lin Zhao, Shao-Ping Lu, Tao Chen, Zhenglu Yang, and Ariel Shamir. 2021. Deep Symmetric Network for Underexposed Image Enhancement with Recurrent Attentional Learning. In *Proceedings of the IEEE/CVF International Conference on Computer Vision*. 12075–12084.

Supplementary Material

A Comparison of Network Parameters

Table A presents a comparison of the number of network parameters. Our method has a slightly higher number of parameters compared to other predefined filter-based methods due to the inclusion of an MLP in our IA-NILUT. However, our method uses fewer parameters than 3DLUTs and AdaInt, which utilize multiple LUTs containing more parameters than our MLP.

B Ablation Study about Sorted RGB Values

In the IA-NILUT, we use the sorted RGB values as described in Eq. (3) of the main paper. To demonstrate the effectiveness of the sorted RGB values, we present the filter effects when the sorted RGB values are not used in Figure A. The color temperature filter is expected to only affect color; however, without the sorted RGB values, it also impacts contrast. This result highlights the importance of the sorted RGB values for each filter to achieve the desired effects.

C Ablation Study about the Prompt Guidance Loss

To further analyze the prompt guidance loss, we exclude the constraints on the untargeted CLIP scores as follows,

$$\mathcal{L}'_{PG} = \sum_{j=1}^J \left(\lambda_j \left| \frac{\partial c_j}{\partial w_j} - 1 \right| \right). \quad (A)$$

We present the effects of filters when training the IA-NILUT with \mathcal{L}'_{PG} in Figure B. When we use \mathcal{L}'_{PG} , all CLIP scores can be changed; therefore, the desired effect is not achieved. This result highlights the significance of our design of the prompt guidance loss.

D Additional Visualizations of Filter Effects

We present additional visualizations of filter effects in Figures C and D, where each filter produces a specific effect associated with the corresponding guiding prompts. We show further examples of sequentially applying predicted parameters in Figures E and F. The enhancement process can be visualized in a way that is easy for humans to understand.

Table A: Comparison of network parameters.

Method	#Network parameters
3DLUTs [31]	593.5 K
AdaInt [29]	619.7 K
CLUTNet [33]	278.7 K
D&R's filters [20]	248.6 K
Exposure's filters [8]	266.0 K
UIE's filters [12]	250.6 K
RSFNet's filters [19]	250.6 K
PG-IA-NILUT (ours)	449.3 K

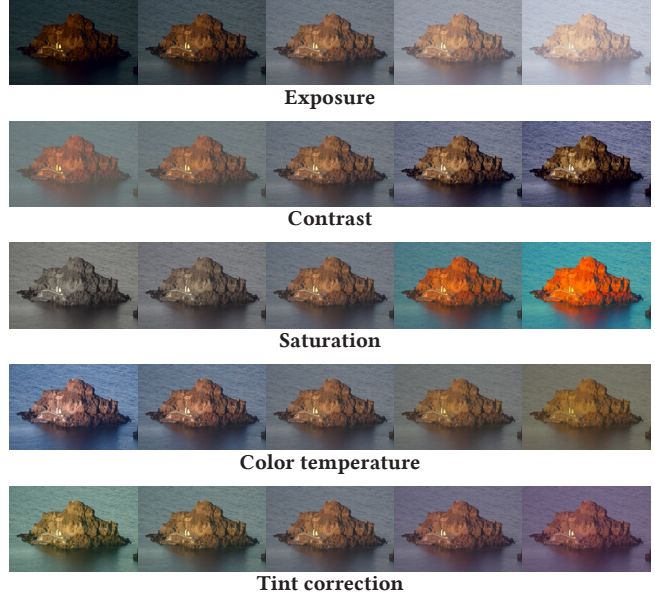


Figure A: Filter effects of the IA-NILUT without the sorted RGB values.

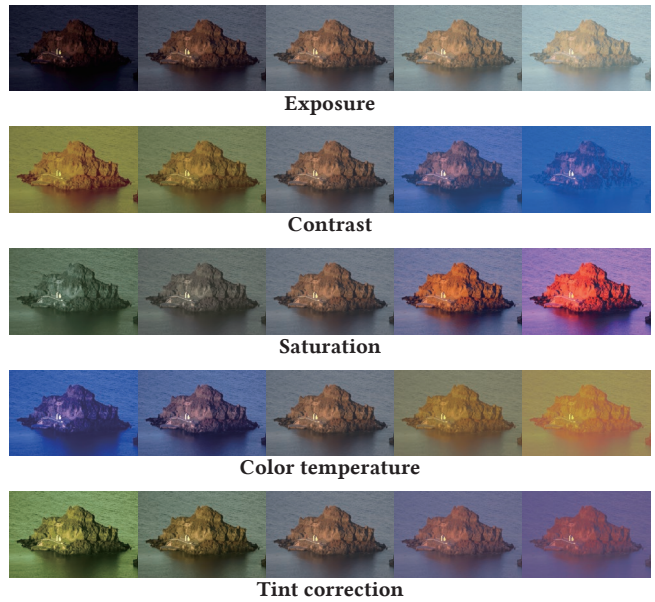


Figure B: Filter effects of the IA-NILUT with \mathcal{L}'_{PG} .

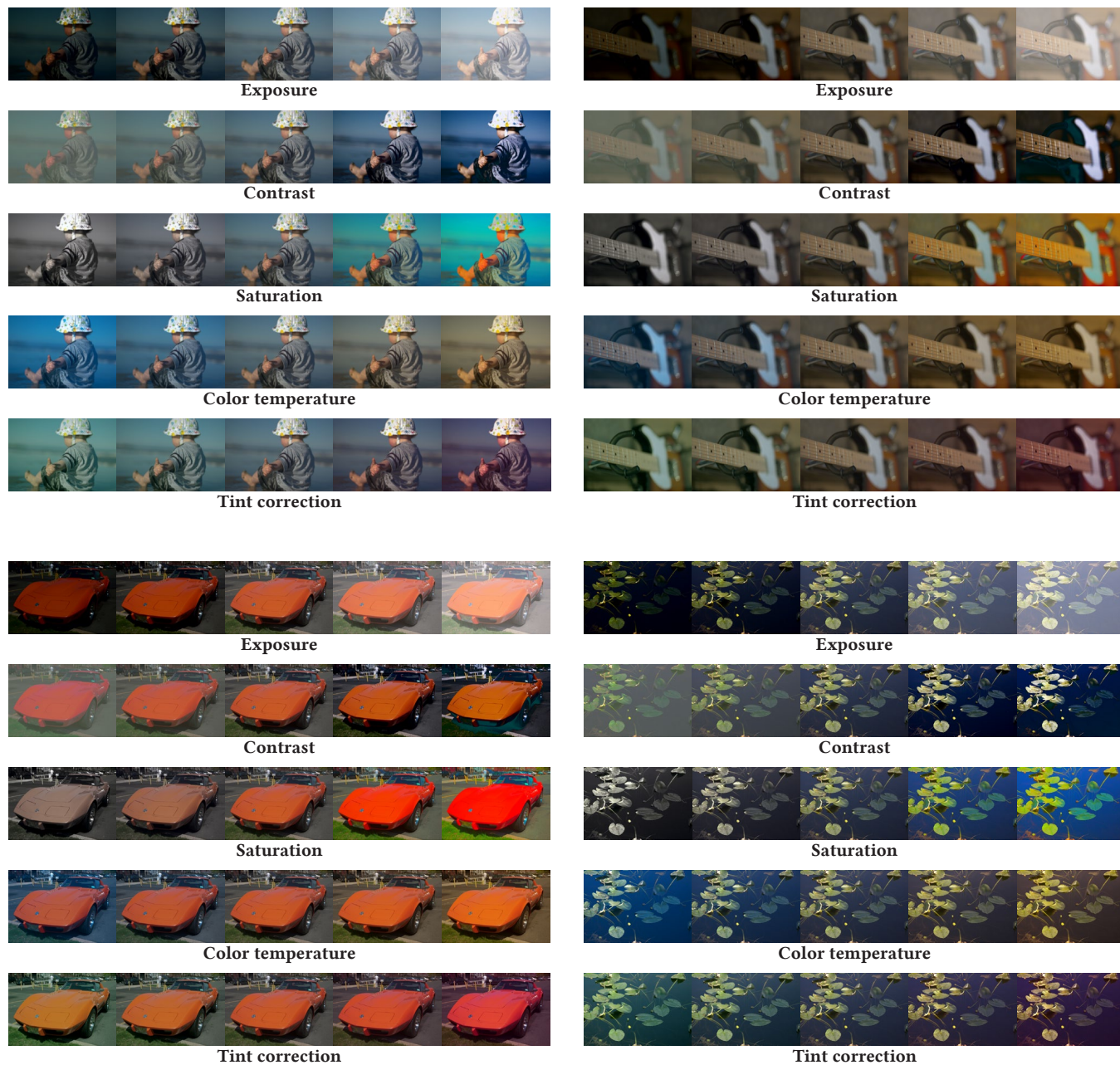


Figure C: Visualization of learned filter effects. Only certain parameters are varied while others are held constant at 0. The images are samples from FiveK.

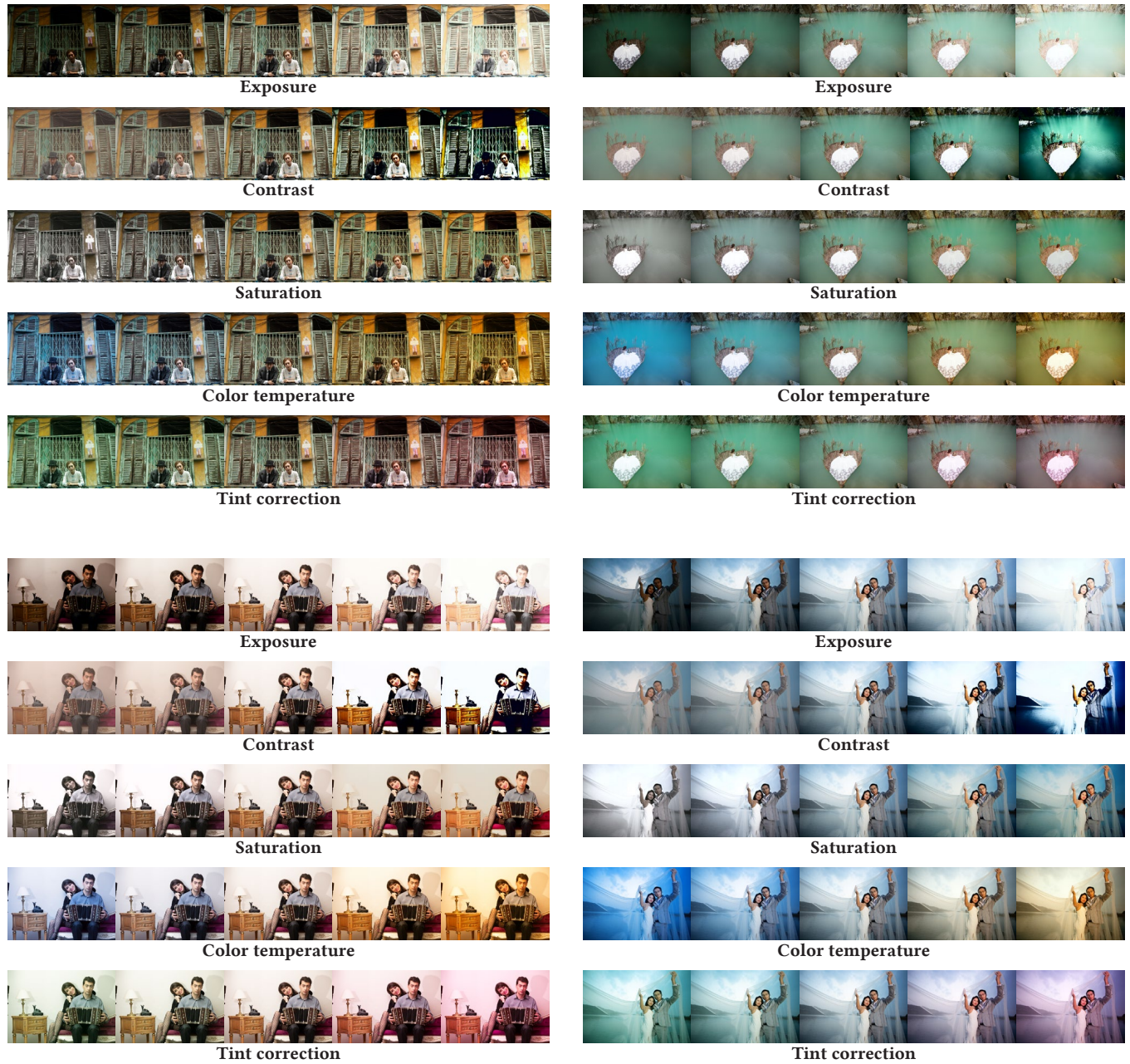


Figure D: Visualization of learned filter effects. Only certain parameters are varied while others are held constant at 0. The images are samples from PPR10K.

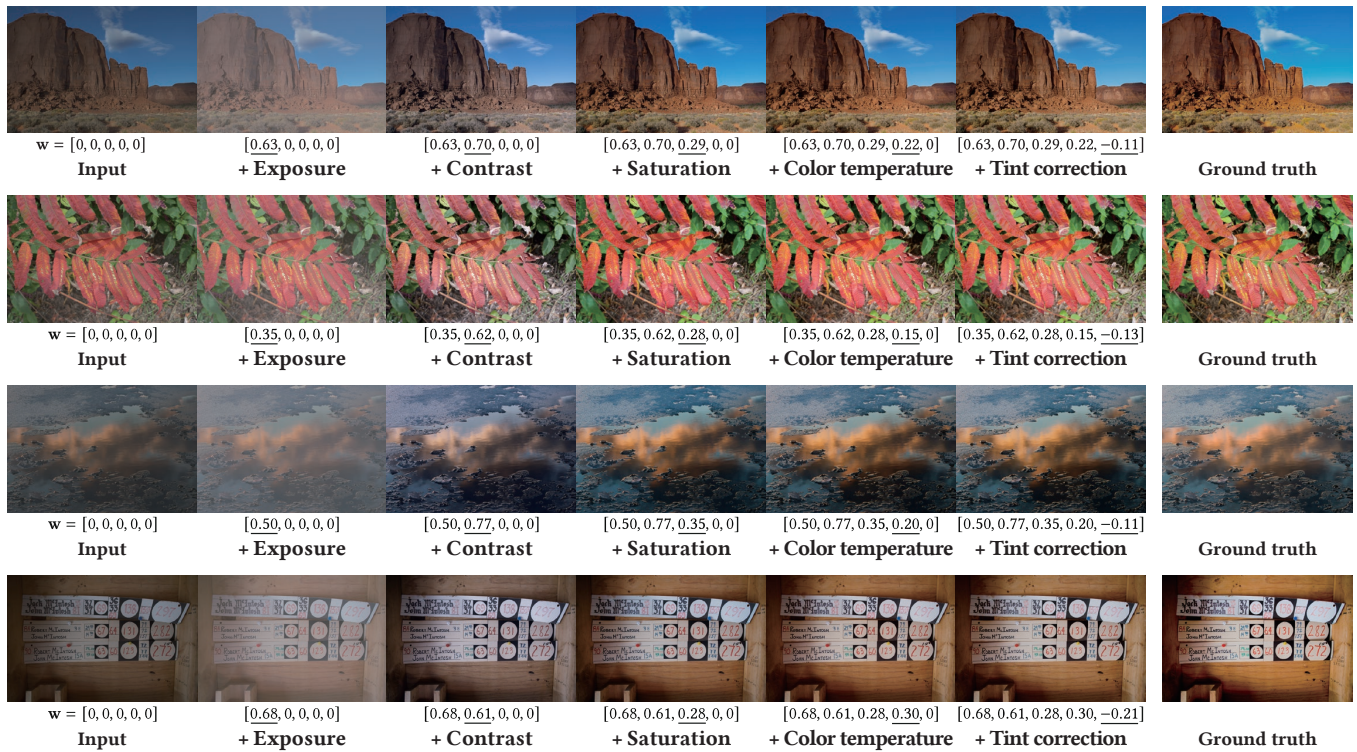


Figure E: Sequential application of predicted parameters. This sequential application is for visualization purposes only, and the all effects are applied simultaneously in practice. The images are samples from FiveK.

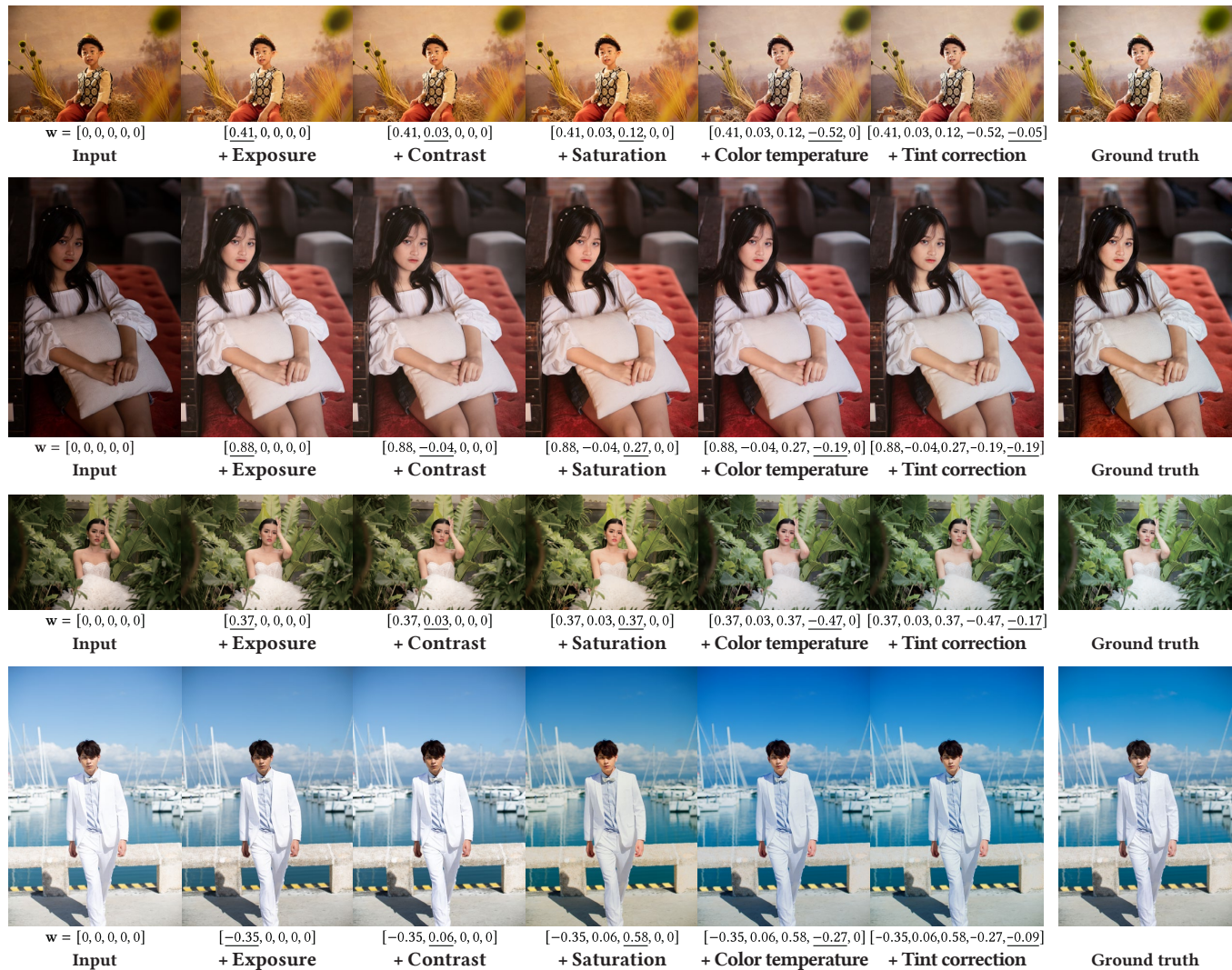


Figure F: Sequential application of predicted parameters. This sequential application is for visualization purposes only, and the all effects are applied simultaneously in practice. The images are samples from PPR10K.